Available online at www.sciencedirect.com
SCIENCE DIRECT®
Ocean Modelling 7 (2004) 75–95
Ocean Modelling
www.elsevier.com/locate/ocemod

Modeling ocean deep convection

V.M. Canuto [a,b,*], A. Howard [a,c], P. Hogan [d], Y. Cheng [a], M.S. Dubovikov [a], L.M. Montenegro [e]

[a] NASA, Goddard Institute for Space Studies, 2880 Broadway, New York, NY 10025, USA
[b] Department of Applied Physics and Mathematics, Columbia University, New York, NY 10027, USA
[c] Department of Earth, Atmospheric and Planetary Sciences, MIT, Cambridge, MA 02139, USA
[d] Naval Research Laboratory, Stennis Space Center, MS 39529, USA
[e] Department of Physics, BCC, CUNY, New York, NY 10453, USA

Abstract

The goal of this study is to assess models for Deep Convection with special emphasis on their use in coarse resolution ocean general circulation models. A model for deep convection must contain both vertical transport and lateral advection by mesoscale eddies generated by baroclinic instabilities. The first process operates mostly in the initial phases while the second dominates the final stages. Here, the emphasis is on models for vertical mixing. When mesoscales are not resolved, they are treated with the Gent and McWilliams parameterization. The model results are tested against the measurements of Lavender, Davis and Owens, 2002 (LDO) in the Labrador Sea. Specifically, we shall inquire whether the models are able to reproduce the region of "*deepest convection*," which we shall refer to as DC (mixed layer depths 800–1300 m). The region where it was measured by Lavender et al. (2002) will be referred to as the LDO region. The main results of this study can be summarized as follows.

(1) $3°\times3°$ *resolution.* A GFDL-type OGCM with the GISS vertical mixing model predicts DC in the LDO region where the vertical heat diffusivity is found to be 10 $m^2\,s^{-1}$, a value that is quite close to the one suggested by heuristic studies. No parameter was changed from the original GISS model. However, the GISS model also predicts some DC in a region to the east of the LDO region.
(2) $3°\times3°$ *resolution.* A GFDL-type OGCM with the KPP model (everything else being the same) does not predict DC in the LDO region where the vertical heat diffusivity is found to be 0.5×10^{-4} $m^2\,s^{-1}$ which is the background value. The KPP model yields DC only to the east of the LDO region.
(3) $1°\times1°$ *resolution.* In this case, a MY2.5 mixing scheme predicts DC in the LDO region. However, it also predicts DC to the west, north and south of it, where it is not observed. The behavior of the KPP and MY models are somewhat anti-symmetric. The MY models yield too low a mixing in stably stratified

* Corresponding author. Address: NASA, Goddard Institute for Space Studies, 2880 Broadway, New York, NY 10025, USA. Tel.: +1-212-6785571; fax: +1-212-6785560.
E-mail address: vcanuto@giss.nasa.gov (V.M. Canuto).

1463-5003/$ - see front matter
doi:10.1016/S1463-5003(03)00038-6

flows since they predict a critical Richardson number $Ri(\mathrm{cr}) = 0.19$ which is five times smaller than the value $Ri(\mathrm{cr}) = \mathrm{O}(1)$ needed to obtain realistic ML depths. However, as discussed above, in unstable stratifications the MY models yield better results. On the other hand, the KPP model, which was motivated primarily by the need to overcome the MY "too low mixing" in stable stratification, yields at coarse resolution, no DC in the LDO region. In this respect, the GISS model, yields both a correct $Ri(\mathrm{cr}) = \mathrm{O}(1)$ in stable stratification and correct results in the unstable configuration in the LDO region.

(4) $1/3^\circ \times 1/3^\circ$ *resolution.* In this case, KPP predicts mixed layer depths up to 1.7 km inside the LDO region where at coarse resolution none existed. However, the model still produces DC at locations outside the LDO region where it is not observed. However, since these regions are intermingled with very shallow mixed layer depths, the resulting mean mixed layer depths turn out to be less than 800 m almost everywhere outside the LDO region.

(5) $1/12^\circ \times 1/12^\circ$ *resolution.* In this case, KPP predicts mixed layer depths up to 3 km both inside and outside the LDO region. These regions are, here too, intermingled with very shallow mixed layer depths with resulting mean mixed depths greater than 800 m both inside and outside the LDO region.

In conclusion, as for a model for deep convection to be used in coarse resolution, these results indicate that the GISS mixing model fares well with observations in both stable and unstable stratifications but overestimates its geographical extent. This leads to the problem of future improvements of the model. It must be generalized to include the following physically important features: (a) *rotation* that becomes important in the later phases of deep convection when it acts to slow down the rate of mixed layer deepening, (b) *non-locality*, in particular skewness which is large (negative) in the initial phases of deep convection and becomes small in the final stages, and finally, (c) a new model to treat *lateral advection* by baroclinic eddies that in the final stages of deep convection dominates over vertical transport.

1. Introduction

Earth's atmosphere interacts with the ocean in two ways. Wind stresses cause strong mixing in the first ~100 m of the ocean (mixed layer, ML) but hardly affect water masses below the ML where lies the largest portion of the ocean characterized by stable stratification and thus weak mixing. To the effect of communicating with the deep ocean, e.g., in the process of absorbing atmospheric CO_2, stable stratification acts like a rigid lid that insulates the strongly mixed ML from the weakly mixed deep ocean. If such a configuration always prevailed, the deep ocean would be shielded from climatic events; deep waters would be dynamically decoupled from surface phenomena and the ocean deep currents would be considerably weaker than what is observed. Differential solar heating between low and high latitudes would not result in a poleward flow of warm waters and the Atlantic would look more like the Pacific where there are no deep convective regions (Weaver et al., 1999). Earth's climate would be quite different from what is observed today.

Deep Convection is the only process through which surface phenomena such as buoyancy losses, brine rejection, etc., pierce the lid of strong stable stratification that characterizes the thermocline. Ultimately, this leads to the formation of deep waters (Chu and Gascard, 1991; Maxworthy, 1997; Marshall and Schott, 1999; The Labrador Sea Deep Convection Experiment,

2002). Open ocean deep convection occurs in a small number of locations, Labrador, Greenland, Weddell and Western Mediterranean Seas, and yet it is one of the ocean's major features since it represents the initial stage of the global-scale ventilation loops of the world ocean (Sander et al., 1995). In fact, it is the dominant mechanism responsible for the production of North Atlantic Deep Water (NADW) and of the Antarctic Bottom Water (AABW, Weaver et al., 1999). Both NADW and AABW play a major role in earth's climate.

Loss of surface buoyancy and/or brine rejection lead to a top-heavy, unstable configuration which acts as precursor of turbulent motion that ultimately leads to deep convection. The latter upwells warmer waters that can melt ice and reduce the albedo resulting in a "negative feedback" that affects climate (Killworth, 1983). Regrettably, however, deep convection is still poorly modeled in coarse resolution OGCM (Killworth, 1989). While laboratory and numerical simulations (Sander et al., 1995; Denbo and Skyllingstad, 1996; Skyllingstad et al., 1996; Maxworthy, 1997; Marshall and Schott, 1999) have brought to light several key features of convective processes, the translation of this information into a reliable model for coarse resolution OGCMs has not yet been achieved but, given the complexity of the phenomenon, this is hardly surprising. Before we test models for deep convection, it is important to discuss some of its key features:

(1) *Deep convection is a highly turbulent process*. This is exhibited by the large vertical diffusivities K_v:

$$K_v \sim \ell w \sim (1\text{–}10)10^5 \ \mathrm{cm^2\,s^{-1}} \tag{1a}$$

where we have used $\ell \sim (1\text{–}2)$ km and $w \sim (1\text{–}5)\ \mathrm{cm\,s^{-1}}$, as discussed by Marshall and Schott (1999). Equivalently, one may consider the large value of the Reynolds number:

$$Re \sim K_v/\nu \sim 10^7 \tag{1b}$$

where $\nu \sim 10^{-2}\ \mathrm{cm^2\,s^{-1}}$ is the kinematic viscosity of seawater. Thus, a high-Re turbulence model is needed to describe deep convective processes.

(2) *Deep convection is affected by rotation*. Consider the characteristic length scale (Golystin, 1980),

$$\ell(\mathrm{rot}) = (B_*/f^3)^{1/2} \sim (0.15\text{–}0.56)\ \mathrm{km} \tag{1c}$$

where B_* is the surface buoyancy and f is the Coriolis parameter. The numerical values in (1c) correspond to the Greenland and Mediterranean Seas (Marshall and Schott, 1999, Table 3.4.1). Contrary to the atmospheric case whose $\ell(\mathrm{rot})$ is much larger than the height $\approx$1 km of the planetary boundary layer, in the ocean case the reverse is often true, namely $\ell(\mathrm{rot})$ may be considerably smaller than the ocean depth H that, for the two cases just cited, is 1.5 and 1.8 km. This yields small Rossby numbers $Ro = \ell(\mathrm{rot})/H = 0.1\text{–}0.3$, an indication of the importance of rotation.

A turbulence model must be able to incorporate rotational effects and more specifically, it must be able to reproduce key features like the Golystin's scale (1c). Rotation enters the turbulence equations not only through the linear Coriolis term in the dynamic equations for the turbulent velocity but, more important, it affects the very structure of the non-linear interactions that are at the heart of turbulence. In the presence of rotation, velocity components with different vectors are rotated by the Coriolis force around different axes that coincide with the directions of the corresponding wave-vectors. Thus, the energy cascade from large to small eddies is inhibited. An

inertial range is still present but only for wave numbers larger than $k(\mathrm{rot})$ where the latter is the inverse of Eq. (1c). For wave numbers $k < k(\mathrm{rot})$, the spectrum is no longer of the Kolmogorov type. That is, one has two regimes:

$$\ell > \ell(\mathrm{rot}) : E(k) \sim (\varepsilon\Omega)^{1/2}k^{-2}, \quad \ell < \ell(\mathrm{rot}) : E(k) \sim \varepsilon^{2/3}k^{-5/3} \tag{1d}$$

where ε is the rate of energy dissipation. Integrating the two spectra, one derives that the corresponding velocities with and without rotation are derived to be

$$w(\mathrm{rot}) \sim [\ell/\ell(\mathrm{rot})]^{1/2}(B_*/f)^{1/2}, \quad w_0 \sim (B_*H)^{1/3} \tag{1e}$$

where we have taken the dissipation rate ε equal to the surface buoyancy flux B_*. Values of $w(\mathrm{rot})$ and w_0 for the Mediterranean, Labrador and Greenland Seas can be found in Table 3.4.1 of Marshall and Schott (1999). A turbulence model capable of predicting the two regimes of the energy spectrum (1d) has recently been constructed and its implications tested against direct numerical simulations (Canuto and Dubovikov, 1997).

(3) *Deep convection cannot be fully represented by a purely local model.* If σ, $1-\sigma$ are the areas occupied by the up/downdrafts (plumes), one has (Moeng and Rotunno, 1990):

$$\sigma = 1/2(1-D), \quad D = S_w(1+S_w^2)^{-1/2}, \quad S_w = \overline{w^3}/\overline{w^2}^{3/2} \tag{2a}$$

where S_w is the skewness of the velocity field. Labrador Sea data (Lavender et al., 2002; Herbaut and Marshall, 2002) show that in the initial stages of convective deepening, S_w is large and negative while in the final stages it is small: skewness subsides with time (for numerical values of S_w, see Table 1 of Lavender et al., 2002). This means that updrafts subside with time and that the downward vertical velocities occur more frequently than upward velocities. By using a local model with $S_w = 0$, or equivalently:

$$\sigma = 1/2 \tag{2b}$$

one assumes that downdrafts and updrafts occupy the same fractional areas, that is, a local model represents only the final stages of deep convection. On the other hand, the OPPS model (Ocean Penetrative Plume Scheme) of Paluszkiewicz et al. (1994), Paluszkiewicz and Romea (1997) represents the initial stages of convective processes. In fact, consider the two assumptions underlying the OPPS; (a) an *isolated plume.* This means that the fractional area occupied by the plume must be small,

$$1-\sigma \ll 1 \tag{2c}$$

From (2a) it follows that S_w must be large and negative and thus a plume model applies only to the initial stages of deep convection; (b) a *quiescent environment* in which the plume is embedded. If

Table 1
Description of the main physical features of the initial and final stages of Deep Convection

	Ω	S_w	NL	LA	PM	TM
Initial stages	No	Yes	Yes	No	Yes	Yes
Final stages	Yes	No	No	Yes	No	Yes

Non-locality (NL), lateral advection due to baroclinic instability (LA), plume model (PM) and turbulence model (TM).

the downward plume's velocity is w_d and the updraft's velocity is w_u, mass conservation demands that:

$$(1-\sigma)/\sigma = w_u/w_d \tag{2d}$$

Since in the initial stages of development downward plumes have velocities some ten times larger than the updrafts, Eq. (2d) implies again (2c). Thus, both assumptions of the OPPS model represent the same physical picture of a plume in the initial stages of development whereas a turbulence model can describe all stages provided it is non-local, that is, capable of incorporating the velocity field skewness S_w.

(4) *Deep convection is not a purely vertical process*. The initial and final stages are characterized not only by different values of the skewness S_w but also by an additional important feature (Jones and Marshall, 1993; Visbeck et al., 1996; Marshall and Schott, 1999; Herbaut and Marshall, 2002; Lavender et al., 2002). In the initial phases, the mixed layer deepens at a rate in accord with that given by vertical mixing models (Visbeck et al., 1996). However, when the plume has deepened to a distance ℓ such that $\ell > \ell(\mathrm{rot})$, rotation takes over and a baroclinic instability sets in. The deepening process is arrested since baroclinic eddies transport fluid masses away laterally. Thus, in the later stages of DC, lateral advection dominates over vertical transport (see Fig. 6 of Visbeck et al., 1996). Since Lavender et al. (2002, Fig. 13) have shown that the heat flux carried by the vertical plumes cannot balance the winter surface heat loss, a considerable fraction of the heat flux must be carried by "features" that have a life time longer than that of the plumes O(hours). In Table 1 we highlight the relative importance of the different processes in the initial and final stages of deep convection.

Since a plume model is applicable mostly in the initial stages of deep convection, it may be difficult to connect it with the initiation of baroclinic instabilities that occur mostly in the final stages (LA and PM columns). On the other hand, a turbulence model valid for arbitrary values of skewness S_w and rotation, is applicable to all stages of deep convection (TM column). In conclusion, a *reliable model for deep convection requires the combination of a vertical mixing turbulence model with rotation and non-locality, together with a mesoscale parameterization to describe lateral advection.*

2. Models of deep convection

2.1. Convective adjustment

Convective Adjustment (CA) was proposed by Bryan (1969) as a temporary model but it is still in use today. It has been recently analyzed by Marotzke (1991) and Marshall and Schott (1999). In the latter study, it was stressed that CA requires an instantaneous adjustment of the water column while in reality the time of mixing t_{mix} is finite (of the order of 12 h or so). Stated differently, the CA adjustment scheme corresponds to an extremely large vertical diffusivity K_v whereas one expects that:

$$K_v \approx h^2/t_{\mathrm{mix}} \approx h w_p \tag{3}$$

Using $w_p = 5$ cm/s and $h = 1$ km, one obtains $K_v \sim 50\ \mathrm{m^2\,s^{-1}}$ (Send and Marshall, 1995). Marotzke (1991) used $K_v = 1\ \mathrm{m^2\,s^{-1}}$ while Klinger et al. (1996) used $K_v = (10\text{–}50)\ \mathrm{m^2\,s^{-1}}$. From the

viewpoint of the consequences of the CA scheme, Bryan (1986) pointed out that the standard GFDL scheme leads to the collapse of the meridional circulation. On the other hand, the collapse is avoided if one employs a complete mixing scheme and/or a treatment of DC as a vertical diffusion (Marotzke, 1991). Reviewing the problem, Paluszkiewicz and Romea (1997) concluded that the CA schemes do not produce realistic vertical density structure, do not create the correct quantity of deep water, and do not use a time scale of adjustment in agreement with tracer ages or observations. Kim and Stossel (2001) have pointed out that CA yields excessive convection that upwells too much heat which in turn yields too little sea-ice cover. Finally, Yin and Sarachik (1994) suggested and tested a scheme that treats DC as a vertical diffusion.

It would be reassuring if a turbulence model could reproduce the values of the vertical diffusivities used in these heuristic models. As we shall show in Fig. 4, this is indeed the case.

2.2. Turbulence models

Conspicuously absent in the treatment of deep convection have been turbulence models, as pointed out by several authors. Killworth (1989) has stated that "while models for the mixed layer dynamic are legion, those for deep convection are rare"; Maxworthy (1997) wrote that: "thus far, turbulence schemes have tended to be restricted to surface and local area modeling" and that "one wants to hope that more complex closure schemes will be tried on problems like deep convection" while Marshall and Schott (1999) state that: "an effort should be made to apply them to these deep convective flows" and that "the challenge for the future is to transform the insights about deep convection into a parametric representation".

This paper is an attempt to fill this gap. Specifically, we assess the MY, KPP and GISS models for the vertical mixing. Lateral advection is modeled with the parameterization of Gent and McWilliams (1990). The data on deep convection are from the Labrador Sea (Lavender et al., 2002). In its present formulation, the GISS model is local (valid in the final stages of evolution, third column in Table 1) and has no rotation. Thus, we expect that the model will overestimate the convective depth as the results presented below will indeed show. In a second study, we shall use the GISS local model (plus the GM model) but with the inclusion of *rotation* in the vertical mixing model. In a third study, we shall include *non-locality* in the GISS model so as to account for both initial and final stages of deep convective processes (lateral advection is still treated with the GM model). In a fourth study, we shall use the GISS model employed in the third study, but the *mesoscale model* will no longer be the Gent-McWilliams model but a new one (Canuto and Dubovikov, submitted for publication) that has been developed and is presently being tested against data from an eddy resolving ocean code.

3. The GISS turbulence model: general features

This vertical mixing model was constructed using the Reynolds stress method (RSM, Canuto et al., 2001a, 2002; cited as C1,2; Cheng et al., 2002). It includes a velocity field and two active scalar fields, temperature and salinity. The model can be time dependent or stationary, local or non-local, with or without rotation. In the stationary and local case, the GISS model becomes an

algebraic set of equations whose solution is analytical. The resulting vertical turbulent fluxes of momentum, heat and salt are given by

$$\overline{u'w'} = -K_{\mathrm{m}}\frac{\partial U}{\partial z}, \quad \overline{w'T'} = -K_h\frac{\partial T}{\partial z}, \quad \overline{w's'} = -K_s\frac{\partial S}{\partial z} \tag{4a}$$

Here, U, T and S are the mean velocity, temperature and salinity. The vertical eddy diffusivities K_α (α stands for momentum, heat and salinity) can be written in two representations

$$K_{\alpha 1} = \Gamma_{\alpha 1}\ell^2\Sigma, \quad K_{\alpha 2} = \Gamma_{\alpha 2}\varepsilon N^{-2} \tag{4b}$$

where the mixing efficiencies Γ_α are given by

$$\Gamma_{\alpha 1} = cS_\alpha(\tau\Sigma)^{-1}, \quad 2\Gamma_{\alpha 2} = S_\alpha(N\tau)^2 \tag{4c}$$

Here, ℓ is the mixing length, ε is the dissipation of turbulent kinetic energy, τ is the eddy turnover time, N is the Brunt–Vaisala frequency, Σ is the mean shear and c is a constant. The *structure functions* S_α are analytic functions of the Richardson number $Ri = N^2/\Sigma^2$ and of the density ratio $R_\rho = \beta\partial S/\partial z(\alpha\partial T/\partial z)^{-1}$ where α and β are the thermal expansion and haline contraction coefficients. Once the heat and salt diffusivities are known, the passive scalar K_c and mass diffusivities K_ρ are also known since

$$K_c = (K_h + R_\rho K_s)(1 + R_\rho)^{-1}, \quad K_\rho = (K_h - R_\rho K_s)(1 - R_\rho)^{-1} \tag{4d}$$

The physical interpretation of the model is as follows. $K_{\alpha 1}$ is the contribution due to wind shear while $K_{\alpha 2}$ is due to internal wave breaking *if no convection is present*. Since these processes coexist, the diffusivity K_α is the sum of the two contributions

$$K_\alpha = K_{\alpha 1} + K_{\alpha 2} \tag{4e}$$

In the ML, where wind shear is much larger than the internal wave breaking contribution, the first term in (4e) dominates; below the ML, where wind shear becomes inefficient (large Ri), the second term in (4e) dominates and thus a smooth transition of processes is assured. When $N^2 < 0$ (*convective regime*), the contribution to $K_{\alpha 2}$ by internal wave breaking becomes negligible and $K_{\alpha 2}$ is predominantly due to convection.

4. Previous tests of the GISS model

Mixed layer and thermocline. The first representation in (4b) was used in C1,2 and by Burchard and Bolding (2001) and Burchard and Deleersnijder (2001). Below the mixed layer and in the absence of deep convection, the most likely source of mixing is the breaking of internal waves. Using the second representation (4b), the value of εN^{-2} ($N^2 > 0$) due to internal waves breaking was taken from (Polzin, 1996).

Convective efficiencies Γ_α. Since their original introduction (Osborn and Cox, 1972), many discussions have concentrated over the values of these convective efficiencies which, without a turbulence model, remain adjustable parameters. Several questions have remained without an answer, for example: (1) are the $\Gamma_{\alpha 2}$ for momentum, heat and salt the same? (2) is it correct to

assume $\Gamma_{\alpha 2} = 1/4$ as often done, when large eddy simulation (LES) data (Wang et al., 1996) yield the much larger value $\Gamma_{\alpha 2} \approx 1$?

The GISS model computes the Γ_α's which were shown to increase strongly near $R_\rho = 0.6$, a prediction that is consistent with the recent observations of a much larger mixing at Barbados ($R_\rho = 0.6$) than at the NATRE location (Ledwell et al., 1998) where $R_\rho = 0.56$. The GISS model also predicts values of $\Gamma_{\alpha 2}$ up to unity, in agreement with LES data (Wang et al., 1996) thus casting doubts about the universality of the commonly used values 0.2–0.25.

NATRE data. $K_{s,h}$ have often been assumed to be the same but the NATRE measurements have shown that $K_h \neq K_s$. Several authors have investigated the influence of double diffusive processes in OGCMs (Zhang et al., 1998; Merryfield et al., 1999). Some authors treated the ratio K_h/K_s as a free parameter, others (Large et al., 1994) employed the relation $K_s = 1.43K_h$ (however, the measurements show that $K_s = 1.43K_hR_\rho^{-1}$). In general, these studies conclude that double diffusion alters substantially the regional distribution of T and S and that salt fingers are more widespread than diffusive convection. Compared with the $K_h = K_s$ case, deep temperature and salinity become larger, the polar heat transport is lowered and the meridional overturning is reduced. Given the heuristic nature of the relation K_S/K_h employed thus far, it is difficult to compare and/or assess the reliability of the ensuing results.

Tests without an OGCM. Since at 400 m depth the diffusivities are only functions of R_ρ, the values of $R_\rho(z)$ measured at the NATRE site (Ledwell et al., 1998) were used to compute the concentration and mass diffusivities from Eq. (4d). Comparison of the GISS model results with the NATRE data was presented in Fig. 9 of C2. Unpublished results from data at Barbados (R.W. Schmitt, Hawaii Ocean Sciences Meeting, Feb. 2002) of a much larger mixing at Barbados than at NATRE, are also in qualitative agreement with the predictions of the model.

Tests with an OGCM. The GISS model was used in a coarse resolution GFDL-type ocean code and the heat, salt, mass and concentration diffusivities at the NATRE location were computed and shown to reproduce the NATRE data quite closely. The T/S profiles in different ocean's sites were also computed and in general they reproduce the Levitus data well. Particularly significant is the better agreement of the T vs. z profile in the Arctic Ocean.

5. Modeling deep convection

5.1. $3^\circ \times 3^\circ$ resolution

We have employed the NCAR-CSM global ocean model (Large et al., 1997; for details, see Appendix A) with a $3^\circ \times 3^\circ$ resolution. The model requires a vertical mixing scheme and employs a GM model to parameterize the mesoscale eddies. We ran two global simulations with two different vertical mixing schemes, the KPP model (Large et al., 1994) and the GISS model discussed above. The monthly surface forcing calculation and all other aspects of the two OGCM runs were identical. To compare the model results with observations, in Fig. 1 we reproduce the results of Lavender et al. (2002). Measurements show that the *deepest convection*, *DC*, one with mixed-layers deeper than 0.8 km, is confined to the fairly small Lavender, Davis and Owens (LDO) region in the western Labrador Sea, Fig. 1. A similar result is presented in Fig. 12 of Pickart et al. (2002). In Figs. 2 and 3, we exhibit the GISS and KPP simulation points found to yield deepest

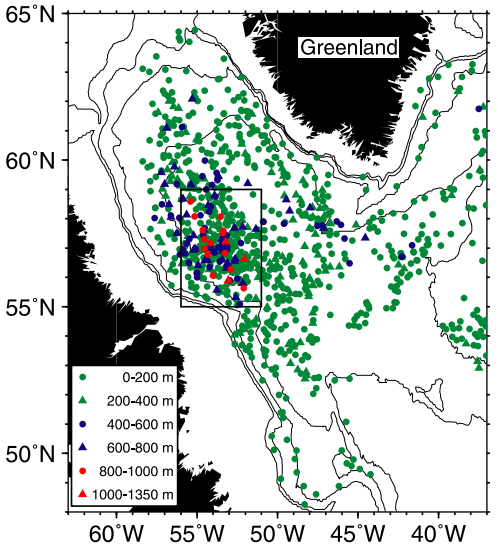

Fig. 1. Mixed layer depths as from Lavender et al. (2002).

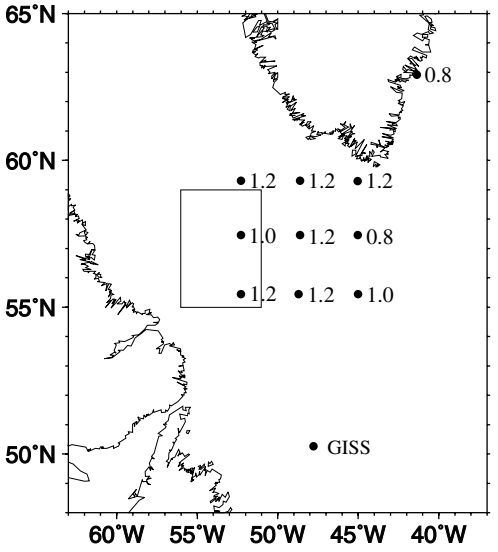

Fig. 2. DC (in km) as from the GISS mixing model.

convection (the results are snapshots taken at March 1 of the 127th year). The GISS mixing model reproduces the deepest convection in the LDO region while the KPP model does not. Within the LDO region, the KPP mixed layers are not deeper than 20 m. Deep convection in the GISS model is evident in both the flat vertical temperature profile and large heat diffusivity down to 1.2 km (Fig. 4). The GISS model heat diffusivity in this column increases from 0.04 $m^2 s^{-1}$ near the surface to a maximum of 6 $m^2 s^{-1}$ at 400 m. In other columns, we find maximum diffusivities up to

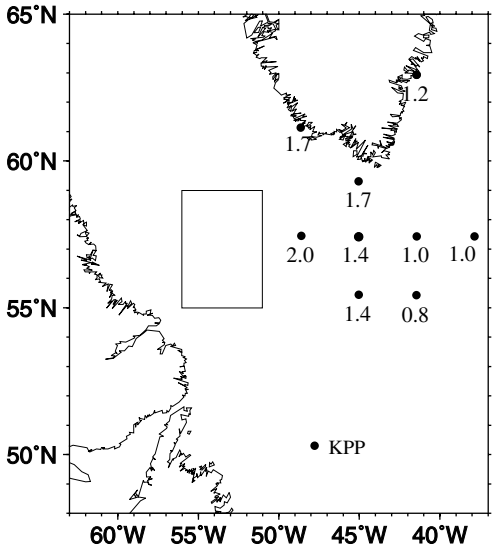

Fig. 3. DC (in km) as from the KPP mixing model.

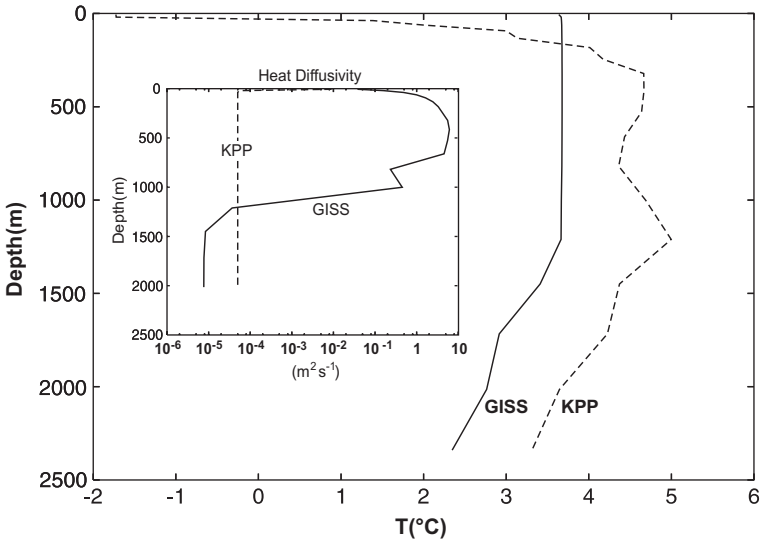

Fig. 4. Profiles of the temperature and heat diffusivity (inset) at 52.2W, 57.5N within the box of Fig. 1.

10 $m^2\,s^{-1}$. The maximum depth attained in the GISS model falls within the observational range while that for the KPP model, which occurs outside the LDO box, is larger than observed. The temperature and diffusivity profiles for the model point 52.2W, 57.5N nearest the center of the "deep convection box", are shown in Fig. 4. In the LDO region, the GISS model diffusivity lies between 1 $m^2\,s^{-1}$ used by Marotzke (1991) and 10–50 $m^2\,s^{-1}$ used by Klinger et al. (1996). At the

points where the KPP model produces deep convection, the diffusivities are of the same order of magnitude as the GISS model, though generally somewhat larger. We also present globally and annually averaged temperature and salinity profiles vs. Levitus data from the 126th model year. Figs. 5 and 6 ought to be compared with Figs. 12 and 13 of C2. The KPP model results are almost unchanged (although very slightly fresher) while the GISS model results are significantly improved. The cool bias of the GISS model vs. observations at and below 1 km has been almost eliminated and the salinity bias between 1 and 3 km has been considerably reduced.

5.2. Sensitivity tests

To investigate the sensitivity of the location of deep convection to model configuration, in particular the landmask, we ran two tests with geographies different from, though less realistic than, the standard case used for the results described above. The addition and subtraction of land points was used as a simple way to perturb the ocean model in order to assess the extent to which the comparison between the different vertical mixing schemes would be affected by an extraneous factor. In each test we altered two points of the landmask while keeping everything else the same.

In test A ("+LAND") we added land to northern Labrador. The two model points at (59.4W, 57.5N) and (59.4W, 59.38N) were converted from 16 level (1.6 km deep) ocean points into land points. The results of test A are shown in Fig. 7a and b. The GISS model has deepest convection

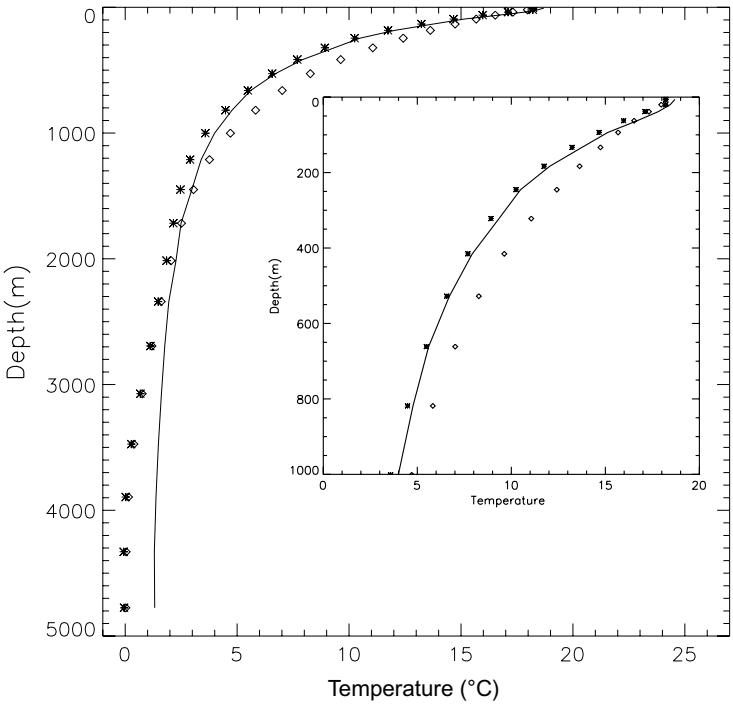

Fig. 5. Global annually averaged temperature vs. depth for both mixing models compared to the Levitus data. Asterisks, GISS model; diamonds, KPP model; solid line, Levitus.

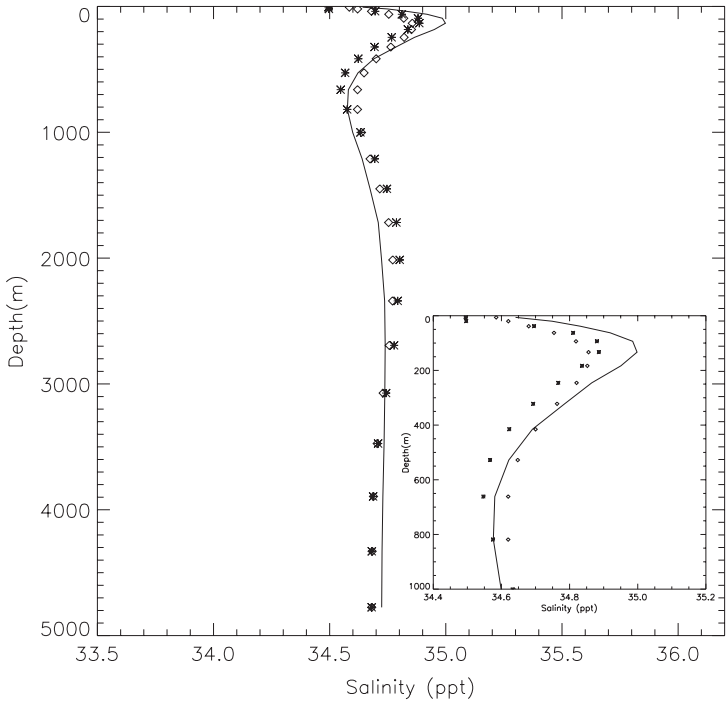

Fig. 6. Global annually averaged salinity vs. depth for both mixing models compared to the Levitus data. Asterisks, GISS model; diamonds, KPP model; solid line, Levitus.

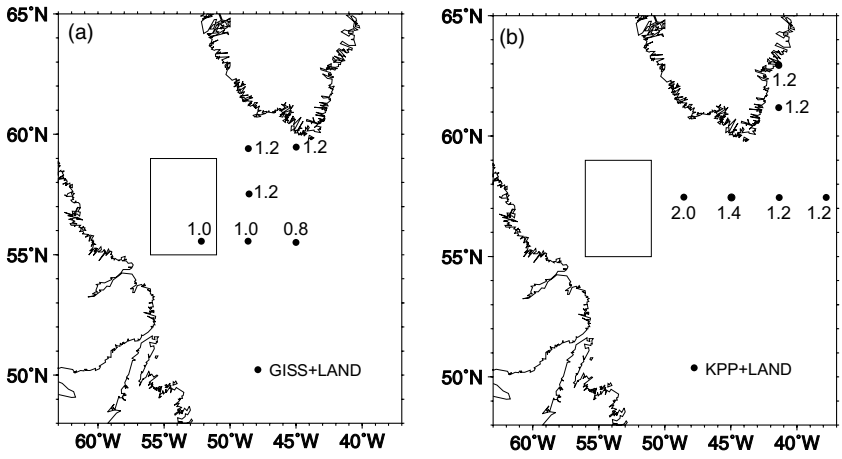

Fig. 7. (a) DC (in km) as from the GISS mixing model. Case + LAND (land added to northern Labrador). (b) DC (in km) as from the KPP mixing model. Case + LAND (land added to northern Labrador).

in fewer spots, one of these still being the southern point of the box where the observations in Lavender et al. (2002) exhibit it, but unlike the standard case, there is no deepest convection in the

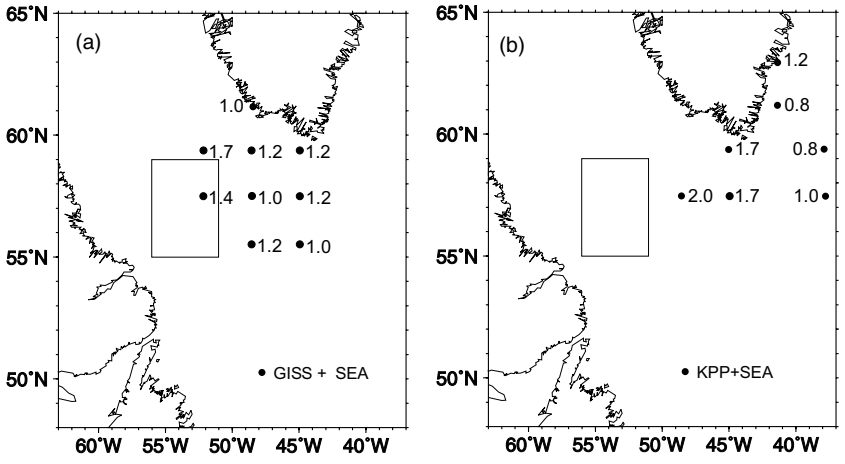

Fig. 8. (a) DC (in km) as from the GISS mixing model. Case + SEA (sea extended southward into Labrador). (b) DC (in km) as from the KPP mixing model. Case + SEA (sea extended southward into Labrador).

north of the box. The KPP also has fewer convection spots, but they still extend over a wide region and yet, no deep convection appears within the box.

In test B ("+SEA") we extended the sea southward into Labrador. The two model points at (59.4W, 55.51N) and (59.4W, 53.42N) were converted from land points into 16 level ocean points. The results of test B are shown in Fig. 8a and b. The GISS model's deepest convection points are now slightly deeper on average and it now has deepest convection in the north of the box, but not in the south. The KPP model's deepest convection moves somewhat to the northeast but there is still no deep convection inside the LDO box. In both tests A–B, no KPP mixed layer inside the LDO box was deeper than 20 m. Although these results show that addition or subtraction of landpoints affects DC, the global results have remained largely unchanged. The ocean basin profiles for the KPP and GISS models in the test A and B cases are very similar to those obtained with the standard landmask and for this reason we do not reproduce them here.

While adding or taking away land degraded the GISS model's performance vis-à-vis the more realistic standard landmask case, it did not improve the KPP model's performance. Furthermore, in both cases the GISS model remained more realistic in having some deepest convection inside the observed box. The qualitative conclusion, robust under change of the landmask for the NCAR CSM ocean model tests, is that both models produce deepest convection in the Labrador Sea area over a larger region than observed but that only the GISS model's deepest convection overlaps the observations.

5.3. 1° × 1° resolution

In this case, the vertical mixing scheme is the MY2.5 model (S. Hakkinen, private communication) and it was used in an ocean model of the northern hemisphere (σ-coordinates with 20 levels with higher resolution near the surface, with monthly forcing, Hakkinen, 1999, 2001). In Fig. 9a and b we present the model results. Fig. 9a corresponds to a forcing from climatology while in Fig. 9b the forcing corresponds to the year 1998. The model produces deepest convection

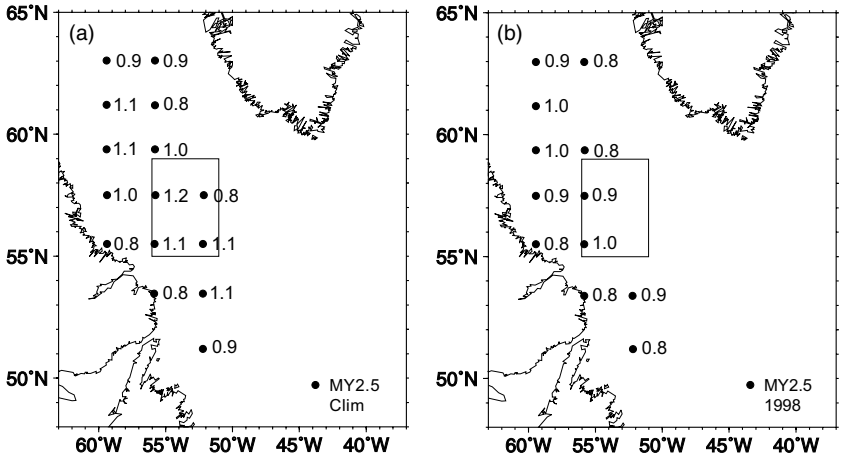

Fig. 9. (a) DC (in km) as from the MY2.5 mixing model. Climatological forcing. (b). DC (in km) as from the MY2.5 mixing model. The forcing corresponds to 1998.

within the LDO region with depths similar to those observed but such regions extend west and much further north and south than observed. The depths in Fig. 9b are somewhat shallower than those in Fig. 9a but the extent of the deepest convection region is almost as large as before.

5.4. 1/3° × 1/3° and 1/12° × 1/12° resolutions

Two more simulations were performed with the hybrid coordinate ocean model (HYCOM; Bleck, 2002). HYCOM is isopycnal in the open, stratified ocean, but using the layered continuity equation makes a dynamically smooth transition to a terrain-following (sigma) coordinate in shallow coastal regions, and to z-level coordinates in the mixed layer and/or unstratified seas. In the North Atlantic HYCOM, the vertical coordinates are configured to allow high vertical resolution (order 15 z-level coordinates in the top 200 m during the winter) in the mixed layer, thereby allowing the use of the KPP closure scheme. The model includes the entire North Atlantic (70°N to 28°S), but only the Labrador Sea is discussed here. There are 26 layers in the vertical, and horizontal resolution is 1/3° (discussed here), and 1/12° (discussed below). The MODAS climatology (Fox et al., 2002) was used to initialize the model and to parameterize the meridional overturning circulation via relaxation to temperature and salinity in 3° buffer zones at the northern and southern boundaries. A monthly climatology formed from the European Centre for Medium Range Forecasting (ECMWF) 10 m reanalysis is used for surface forcing. Bulk formulae were used to calculate the surface heat flux from the net radiation flux, the air temperature, the specific air humidity, the scalar wind speed, and the model's surface (layer 1) temperature. Using the model's SST (instead of climatological SST) tends to self correct the net surface heat flux, i.e., if the SST is too warm the heat flux will decrease and vice versa.

For ease of comparison, the results corresponding to March 1 from the HYCOM simulations were binned in 2.5° squares centered on the same grid points as the NCAR-CSM results shown in Figs. 2 and 3. The maximum mixed layer depth within each bin that exceeds 800 m is shown in Fig. 10a, and the mean mixed layer depth of each bin (greater than 800 m) is shown in Fig. 10b.

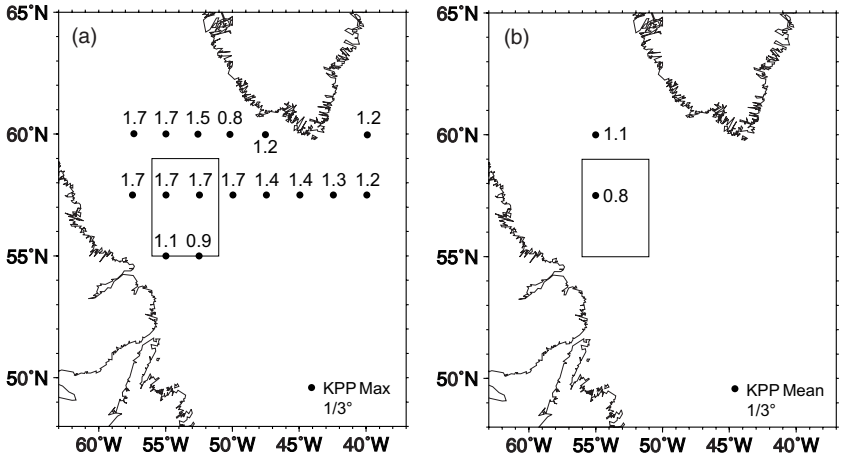

Fig. 10. (a) The maximum (larger than 0.8 km) mixed layer depths (in km) (within a 3° box) predicted by KPP (HYCOM 1/3° × 1/3° resolution ocean code). Forcing is with monthly ECMWF winds and thermal fields. (b) Same as in (a) but for the mean mixed layer depths (within a 3° box).

In HYCOM, the mixed layer depth is defined as the minimum depth where the σ_Θ change from the surface downward corresponds to a 0.2 °C temperature change. Overall, the maximum mixed layer depths are deeper than those observed as shown in Fig. 1, and the distribution of the maxima is not consistent with the observations. There are only two mean mixed layer depth bins $\geqslant$ 800 m (deepest convection), but their locations are consistent with the outlined LDO region (Fig. 10b). In HYCOM with KPP, the deep mixed layers are often spatially uncorrelated, i.e., there can be a 1500 m deep mixed layer and 100 m deep mixed layer at adjacent grid points. This is apparently caused by the magnification of small scale horizontal numerical noise by the mixed layer model. This may be due to the one-dimensional nature of KPP, but other factors, such as how mesoscale ocean features respond to large scale atmospheric forcing, may also play a role. The result, however, is that on this particular (climatological) day, the mean mixed layer depths are heavily influenced by a larger number of "shallow" mixed layer depths within each bin, thereby decreasing the number of bins that meet the 800 m minimum threshold (the region of *deepest convection* as defined earlier).

5.5. 1/12° × 1/12°

The 1/3° HYCOM model described in the previous section was run with an horizontal resolution of 1/12° (about 4.7 km at 58°N). The maximum and mean mixed layer depths in the 2.5° bins are shown in Fig. 11a and b, respectively. As with the 1/3° results, there are more maximum mixed layer depths than mean mixed layer depths, for the reasons described above. However, in the 1/12° model, the mixed layer depths are much deeper than in the 1/3° case. The range of the mean mixed layer depths (Fig. 11b) is 0.8–1.7 km. These depths are consistent with the observations, although most of the deep convection sites lie to the south–east of the observed *deepest convection* sites (Fig. 1). The maximum mixed layer depths (Fig. 11a) are much deeper than those observed, with several of the order of 3 km. They are also more widely distributed than observed.

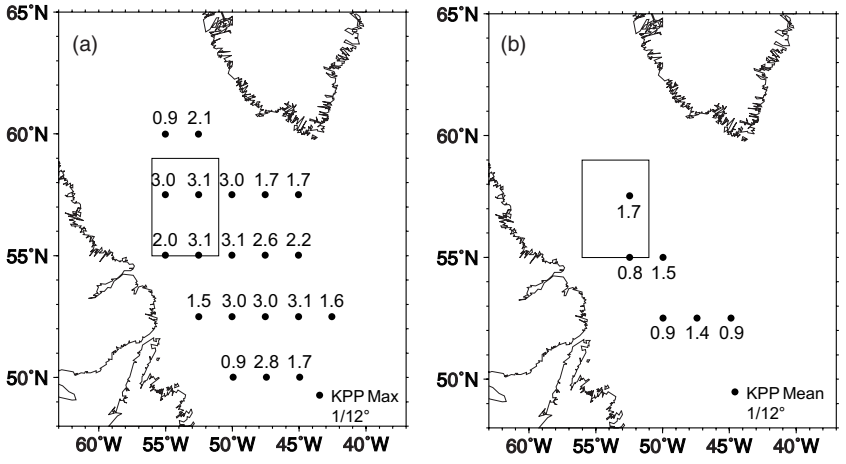

Fig. 11. (a) Same as in Fig. 10a with a 1/12°×1/12° resolution. (b) Same as in Fig. 10b with a 1/12°×1/12° resolution.

This may be due to limitations in how KPP parameterizes deep convective turbulent boundary layers and/or due to other factors such as HYCOM's hybrid coordinate or more inertial currents that give rise to higher current shears.

6. Improvements on the GISS model

6.1. Rotation

As we have already discussed, this is the first in a series of studies of DC that we have planned. Here, we have assessed the performance of a local model for vertical mixing plus a GM model for the mesoscale eddies. The inclusion of rotation in the vertical mixing model will be as follows. In the one-point closure model that we employ, rotation enters in two ways: through the Coriolis force that comes in linearly in the equations and into the pressure-correlations (Canuto et al., 2001a). Such pressure correlations depend on shear $2S_{ij} = U_{i,j} + U_{j,i}$ and vorticity $2V_{ij} = U_{i,j} - U_{j,i}$, where U_i is the mean velocity field and $U_{i,j} = \partial U_i/\partial x_j$. In the presence of Ω, the V_{ij} change to

$$V_{ij} \to V^*_{ij} = V_{i,j} - \varepsilon_{ijk}\Omega_k \tag{5a}$$

where ε_{ijk} is the totally antisymmetric tensor. Since V_{ij} enters in all turbulence equations, both the heat and the momentum fluxes (Reynolds stresses) are affected by rotation $\Omega = (0, \Omega_y, \Omega_z)$, where $\Omega_{y,z} = \Omega(\cos\varphi, \sin\varphi)$, φ being the latitude. The dynamic equations for the heat fluxes and the Reynolds stresses in the presence of Ω have recently been derived. In the local limit, they become an algebraic system that we have already solved. As an example, the first of (4a) now contains additional terms of the form:

$$A\Omega\cos\varphi + B\Omega\sin\varphi \tag{5b}$$

where φ is the latitude. A similar structure also enters the heat flux.

6.2. Non-locality

For a vertical mixing model to be valid both at the beginning and at the end of the DC process, one must allow arbitrary values of the skewness S_w which, as Eq. (2a) shows, is a third-order moment (TOM). Non-local terms appear in both the equation for the heat flux as well as in that of the Reynolds stresses. Before we discuss how to model the TOMs, we note that in the non-local case, Eq. (4a) changes to

$$\overline{u'w'} = -K_{\mathrm{m}}\partial U/\partial z + \gamma_{\mathrm{m}}, \quad \overline{w'T'} = -K_h\partial T/\partial z + \gamma_h \tag{6a}$$

While these expressions are not new, previous authors (e.g., Large et al., 1994) had to employ heuristic models for the γ's and for lack of data, had to take $\gamma_{\mathrm{m}} = 0$. On the other hand, a turbulence model provides the γ's in terms of the TOMs, e.g.:

$$\gamma_h \sim \frac{\partial}{\partial z}\overline{w'^2T'} + A\frac{\partial}{\partial z}\overline{w'T'^2} \tag{6b}$$

Physically, the first term represents the flux of the heat flux while the second term represents the flux of the temperature variance. The presence of the γ's shows that turbulence generates and transports fluxes. Thus, a flux at a given site need not have been generated locally; it may be the result of the transport of a flux generated elsewhere, that being the meaning of non-locality. Heuristic expressions for the TOMs were employed for many years until Moeng and Wyngaard (1989) showed that they provide a very poor representation of the TOMs obtained from LES. Motivated by that result, a new expression for the TOMs was derived (Canuto et al., 1994) by solving their dynamic equations. The results were tested with good results against three sets of LES data for a convective PBL. Recently, a new expression for the TOMs has been derived (Canuto et al., 2001b) which is more compact than the 1994 one. When compared with a new set of LES data for the planetary boundary layer PBL (Mironov et al., 2000), it yields results that are superior to those in 1994. However, ocean TOMs are not the same as those for the PBL. In fact, since earth's rotation influences the dynamics of ocean DC, the TOMs must depend on Ω. To derive the new TOMs(Ω), we shall employ the methodology used in the two previous models for the TOMs. The new TOMs(Ω) will first to be tested against new LES data that include rotation.

6.3. Mesoscale modeling

In principle, mesoscale eddies affect both the heat/salt fluxes as well as momentum fluxes (Reynolds stresses). Since the Gent and McWilliams model (1990) was devised for scalar fluxes, the Reynolds stresses are still modeled through a Fickian diffusion. Improvements of the GM model are difficult since the model was not derived from a set of dynamic equations. However, starting from the Navier–Stokes equations and the equation for a passive scalar, Canuto and Dubovikov (submitted for publication) have recently derived a model whereby the mesoscale effect on both the mean momentum equations and on the equations for scalars can be computed. Some key new features of the new model are as follows:

(1) the bolus velocity contains two terms, the first of which is the downgradient of the potential vorticity rather than the mean thickness as suggested by several authors (e.g., Treguier, 1999),

(2) the second term depends on the mean velocity field **u** and is not present in any of the parameterizations discussed thus far in the literature. The existence of a new term was first suggested by Bryan et al. (1999) but no specific form was derived for it.
(3) since **u** varies with depth, the new term causes a shearing force that erodes the coherence of the eddy field,
(4) thus far, the mesoscale diffusivity κ_m was treated either as an adjustable parameter or dealt with using a heuristic model (Visbeck et al., 1997). The new model expresses κ_m in terms of the large scale (resolved) fields and thus κ_m can be computed. It is predicted to be larger at the surface than in the interior, in agreement with recent heuristic models (Visbeck et al., 1997; Karsten and Marshall, 2002).

7. Conclusions

Since our goal was to investigate models for deep convection to be used in coarse resolution OGCMs, we have analyzed three vertical mixing models. Considering them in the historical order in which they appeared, we have discussed: (a) MY2.5, (b) KPP and (c) GISS model.

(a) as discussed in Canuto et al. (2001a,b, 2002), in stably stratified situations, the MY models produce too shallow mixed layers, a point first made by Martin (1985). Technically, this is due to the fact that the MY models predict a critical Richardson number $Ri(\mathrm{cr}) = 0.19$ which is five times smaller than the value needed to obtain correct mixed layer depths. In an unstably stratified configuration, such as the one characterizing deep convection, the MY models perform better, as shown in Fig. 9. However, since a mixing model is supposed to be applicable everywhere, the shortcomings of the MY models in stable situations must still be amended.
(b) the KPP model was constructed primarily to alleviate the "too little mixing" problem of the MY models. It is interesting to compare its performance vis-à-vis the MY models: KPP yields correct mixed layer depths in stable situations but, *at coarse resolution*, it produces too little mixing in the LDO region (Figs. 3 and 4). However, as the resolution increases, the situation is more complex, as Figs. 10 and 11 show.
(c) since the GISS model predicts $Ri(\mathrm{cr}) \approx \mathrm{O}(1)$, it gives rise to mixed layer depths in stable situations in agreement with the data (Burchard and Bolding, 2001; Burchard and Deleersnijder, 2001). At the same time, in unstable convective-like situations, the predictions for the mixed layer depths are closer to the LDO data than those of the other two models. In so doing, it avoids the shortcomings of both MY and KPP models.

The GISS model is still missing two important ingredients, however. The first is *rotation*. The Reynolds stress method on which the GISS model is based, has definite prescriptions to include the effect of Ω. The new rotation-dependent diffusivities have already been derived (in the local limit) and they will be used next. The second missing ingredient is *non-locality* (counter-gradients) represented by TOMs like the velocity skewness that characterizes the topology of the descending and ascending plumes and for which measurements are available to test the model results. Heuristic models cannot compute the TOMs (which must be borrowed from other sources) while the RSM offers a well defined procedure. Considerable work to derive analytic expressions for the

TOMs has already been done (Canuto et al., 1994, 2001a,b, submitted for publication) and their inclusion in a DC model is now possible.

Thirdly, in both KPP and GISS schemes, lateral advection that dominates the final stages of deep convection has thus far been modeled using the heuristic Gent-McWilliams parameterization. Recent work (Canuto and Dubovikov, submitted for publication) has shown that a mesoscale model can be derived from the basic dynamic equations (Navier–Stokes and scalar equations). The new model will hopefully improve the traditional GM model. The new model has however not yet been independently tested. When that is done and if significant improvements over the GM model will emerge, the lateral advection part of the DC model will also be improved.

Acknowledgements

The authors would like to thank Dr. K.L. Lavender for providing Fig. 1 and granting us permission to reproduce it and Dr. S. Hakkinen for providing us the data to construct Fig. 9. The NASA-GISS authors would like to thank the NASA Climate Program and the NASA Oceanography Program managed by Tsengdar Lee and Eric Lindstrom for financial support. A. Howard and M.S. Dubovikov would like to thank the Physical Oceanography Division of NSF for partial financial support for this study (NSF OCE-0241668).

Appendix A. Numerical scheme

The OGCMs were integrated for 126+ momentum years. In C1-2, for the first 96 years, a depth acceleration was used so that the tracer timestep increased from 10 times the momentum timestep at the surface to 100 times the momentum timestep in the abyss. We have recently found that using the surface tracer timestep throughout the column for the first 96 years makes a noticeable improvement in our model, in which the deep ocean diffusivities vary, though not in the KPP model with constant background diffusivities. In Large et al. (1997), the code was run with the last 30 years of the simulations using a tracer timestep equal to the momentum timestep. However, Kamenkovich et al. (2002) have shown that use of a depth-independent tracer acceleration factor of 12 did not degrade results vis-à-vis use of equal time-steps in the MOM2 ocean component of their climate model; we have found, in a trial with the NCOM, negligible difference in the basin-averaged temperature and salinity profiles between a run in which the last 30 years used a depth-independent tracer acceleration of a factor of 10 and one in which the last 30 years were run synchronously. The results reported here for both the KPP and GISS models accordingly use a tracer timestep 10 times the momentum timestep throughout the ocean for the entire 126-year run. In the simulations C1-2, an artificial cap of 0.1 $m^2 s^{-1}$ was placed on the diffusivities calculated by the GISS model due to fears of numerical instability that turned out to be unfounded. For the runs reported here, the cap was raised to 100 $m^2 s^{-1}$, a limit which was rarely reached in the simulation and which is larger than the diffusivities predicted for the Labrador Sea. With the exceptions of the changes in timestep and GISS mixing model, the OGCM code was the same as in C2.

References

Bleck, R., 2002. Ocean Model. 4, 55.
Bryan, F., 1986. Nature 323, 301.
Bryan, K., 1969. J. Comput. Phys. 4, 347.
Bryan, K., Dukowicz, J.K., Smith, R.D., 1999. J. Phys. Ocean. 29, 2442.
Burchard, H., Bolding, K., 2001. J. Phys. Ocean. 31, 1943.
Burchard, H., Deleersnijder, E., 2001. Ocean Model. 3, 33.
Canuto, V.M., Dubovikov, M.S., 1997. Phys. Fluids 9, 2132.
Canuto, V.M., Dubovikov, M.S., submitted for publication. Ocean Model.
Canuto, V.M., Minotti, F., Ronchi, C., Ypma, R.M., 1994. J. Atmos. Sci. 51, 1605.
Canuto, V.M., Howard, A., Cheng, Y., Dubovikov, M.S., 2001a. J. Phys. Ocean. 31, 1413.
Canuto, V.M., Cheng, Y., Howard, A., 2001b. J. Atmos. Sci. 58, 1169.
Canuto, V.M., Howard, A., Cheng, Y., Dubovikov, M.S., 2002. J. Phys. Ocean. 32, 240.
Canuto, V.M., Cheng, Y., Howard, A., submitted for publication. J. Atmos. Sci.
Cheng, Y., Canuto, V.M., Howard, A., 2002. J. Climate. 8, 2967.
Chu, P.C., Gascard, J.C., 1991. Deep Convection and Deep Water Formation in the Oceans. Elsevier, New York. p. 397.
Denbo, D.W., Skyllingstad, E.D., 1996. J. Geophy. Res. 101, 1095.
Fox, D.N., Teague, W.J., Barron, C.N., Carnes, M.R., Lee, C.M., 2002. Atmos. Ocean Tech. 19, 240.
Gent, P.R., McWilliams, J.C., 1990. J. Phys.Ocean. 20, 150.
Golystin, G.S., 1980. Dokl. Akad. Nauk SSSR 251, 1356.
Hakkinen, S., 1999. J. Geophys. Res. 104, 10991.
Hakkinen, S., 2001. J. Geophys. Res. 106, 13837.
Herbaut, C., Marshall, J., 2002. J. Phys.Ocean. 32, 545.
Kamenkovich, I.V., Sokolov, A.P., Stone, P.H., 2002. Clim. Dynam. 19, 585.
Karsten, R.H., Marshall, J., 2002. J. Phys. Ocean. 32, 3315.
Killworth, P.D., 1983. Rev. Geophys. Space Phys. 21, 1.
Killworth, P.D., 1989. In: Muller, P., Henderson, D. (Eds.), Proc. Aha Huliko'a Hawaiian Winter Workshop. Hawaiian Inst. Geophys. Univ., Hawaii, pp. 59–74.
Kim, S.J., Stossel, A., 2001. J. Phys. Ocean. 31, 650.
Klinger, B., Marshall, J., Send, U., 1996. J. Geophy. Res. 101, 18175.
Jones, H., Marshall, J., 1993. J. Phys. Ocean. 23, 1009.
Large, W.G., McWilliams, J.C., Doney, S.C., 1994. Rev. Geophys. 32 (4), 363.
Large, W.G., Danabasoglu, G., Doney, S.C., McWilliams, J.C., 1997. J. Phys. Ocean. 27, 2418.
Lavender, K.L., Davis, R.E., Brechner Owens, W., 2002. J. Phys. Ocean. 32, 511.
Ledwell, J.R., Watson, A.J., Law, C.S., 1998. J. Geophy. Res. 103, 21499.
Marotzke, J., 1991. J. Phys. Ocean. 21, 903.
Marshall, J., Schott, F., 1999. Rev. Geophys. 37, 1.
Martin, P.J., 1985. J. Geophys. Res. 90, 903.
Maxworthy, T., 1997. Ann. Rev. Fluid Dynam. 29, 327.
Merryfield, W.J., Holloway, G., Gargett, A.E., 1999. J. Phys. Ocean. 29, 1124.
Mironov, D.V., Gryanick, V.M., Moeng, C.H., Olbers, D.J., Wranke, T.H., 2000. Q. J. Roy. Meteor. Soc. 126, 477.
Moeng, C.H., Wyngaard, J.C., 1989. J. Atmos. Sci. 46, 2311.
Moeng, C.H., Rotunno, R., 1990. J. Atmos. Sci. 47, 1149.
Osborn, T.R., Cox, C.S., 1972. Geophys. Fluid Dynam. 3, 321.
Paluszkiewicz, T., Garwood, R.W., Denbo, D.W., 1994. Oceanography 7, 37.
Paluszkiewicz, T., Romea, R.D., 1997. Dynam. Atmos. Oceans 26, 95.
Pickart, R.S., Torres, D.J., Clarke, R.A., 2002. J. Phys. Ocean. 32, 428.
Polzin, K., 1996. J. Phys. Ocean. 26, 1409.
Sander, J., Wolf-Gladrow, D., Olbers, D., 1995. J. Geophy. Res. 100, 20579.

Send, U., Marshall, J., 1995. J. Phys. Ocean. 25, 855.
Skyllingstad, E.D., Paluszkiewicz, T., Denbo, D.W., Smyth, W.D., 1996. Physica D. 98, 574.
The Labrador Sea Deep Convection Experiment, 2002. J. Phys. Ocean. 32 (February Issue).
Treguier, A.M., 1999. J. Mar. Res. 57, 89.
Visbeck, M., Marshall, J., Jones, H., 1996. J. Phys. Ocean. 26, 1721.
Visbeck, M., Marshall, J., Haine, T., Spall, M., 1997. J. Phys. Ocean. 27, 381.
Wang, D., Large, W.G., McWilliams, J.C., 1996. J. Geophy. Res. 101, 3649.
Weaver, A.J., Bitz, C.M., Fanning, A.F., Holland, M.M., 1999. Ann. Rev. Earth Planet Sci. 27, 231.
Yin, F.L., Sarachik, E.S., 1994. J. Phys. Ocean. 24, 1425.
Zhang, J., Schmitt, J.R., Huang, R.X., 1998. J. Phys. Ocean. 28, 589.